Article

pubs.acs.org/Biomac

Glyco-Nanoparticles with Sheddable Saccharide Shells: A Unique and Potent Platform for Hepatoma-Targeting Delivery of Anticancer Drugs

Wei Chen,[†,‡] Yan Zou,[†] Fenghua Meng,[†] Ru Cheng,[†] Chao Deng,*[,†] Jan Feijen,[†,‡] and Zhiyuan Zhong*[,†]

[†]Biomedical Polymers Laboratory, and Jiangsu Key Laboratory of Advanced Functional Polymer Design and Application, Department of Polymer Science and Engineering, College of Chemistry, Chemical Engineering and Materials Science, Soochow University, Suzhou, 215123, People's Republic of China

[‡]Department of Polymer Chemistry and Biomaterials, Faculty of Science and Technology, MIRA Institute for Biomedical Technology and Technical Medicine, University of Twente, P.O. Box 217, 7500 AE Enschede, The Netherlands

Supporting Information

ABSTRACT: Reduction-sensitive shell-sheddable glyco-nanoparticles were designed and developed based on poly(ε-caprolactone)-*graft*-SS-lactobionic acid (PCL-*g*-SS-LBA) copolymer for efficient hepatoma-targeting delivery of doxorubicin (DOX). PCL-*g*-SS-LBA was prepared by ring-opening copolymerization of ε-caprolactone and pyridyl disulfide carbonate followed by postpolymerization modification with thiolated lactobionic acid (LBA-SH) via thiol-disulfide exchange reaction. The dynamic light scattering (DLS) and transmission electron microscopy (TEM) showed that PCL-*g*-SS-LBA was self-assembled into monodisperse nanoparticles (SS-GNs) with a mean diameter of about 80 nm. SS-GNs while remaining stable under physiological conditions (37 °C, pH 7.4) were prone to rapid shell-shedding and aggregation in the presence of 10 mM dithiothreitol (DTT). DOX was loaded into SS-GNs with a decent loading content of 12.0 wt %. Notably, in vitro release studies revealed that about 80.3% DOX was released from DOX-loaded SS-GNs in 24 h under a reductive condition while low drug release (<21%) was observed for DOX-loaded PCL-*g*-LBA nanoparticles (reduction-insensitive control) under otherwise the same condition and for DOX-loaded SS-GNs under a nonreductive condition. The flow cytometry and confocal microscopy observations indicated that SS-GNs were efficiently taken up by asialoglycoprotein receptor (ASGP-R)-overexpressing HepG2 cells likely via a receptor-mediated endocytosis mechanism and DOX was released into the nuclei of cells following 4 h incubation. MTT assays showed that DOX-loaded SS-GNs exhibited a high antitumor activity toward HepG2 cells, which was comparable to free DOX and about 18-fold higher than their reduction-insensitive counterparts, while blank SS-GNs were nontoxic up to a tested concentration of 1.0 mg/mL. These shell-sheddable glyco-nanoparticles are promising for hepatoma-targeting chemotherapy.

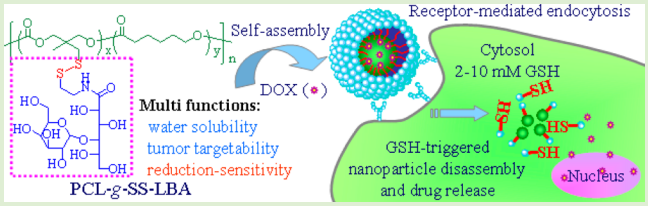

INTRODUCTION

Biodegradable polymeric micelles and nanoparticles have attracted growing attention based on their potential applications in cancer therapy.[1−4] These systems could dramatically improve the bioavailability of anticancer drugs by enhancing drug water solubility, prolonging drug blood circulation time, and improving drug accumulation at tumor tissue via the enhanced permeability and retention (EPR) effect.[5,6] However, despite the fact that significant progress has been made in the past decade, few nanoparticulate drug systems have achieved optimal therapeutic outcomes due to inefficient tumor cell uptake and poor intracellular drug release.[7−9]

The cellular uptake of nanoparticulate drugs can be improved by installing an active targeting ligand.[10,11] Taking advantage of hepatocellular carcinoma cells overexpressing asialoglycoprotein receptors (ASGP-R), saccharides such as β-D-galactose (Gal), *N*-acetylgalactosamine, and lactose-functionalized nanoparticles have been designed for targeted liver cancer therapy.[12−14] Notably, glycopolymers with a high saccharide density are found to result in markedly improved binding affinity toward proteins due to the presence of polyvalent interactions (known as cluster glycoside effect).[15−17] Yang et al. demonstrated that micelles self-assembled from Gal-functionalized amphiphilic polycarbonate block copolymers exhibited efficient cellular uptake and significantly increased antitumor activity in ASGP-R positive HepG2 cells as compared to HEK293 cells.[18]

The intracellular release of drugs has shown to be facilitated using bioresponsive, in particular, pH and redox-responsive, degradable nanocarriers.[19−22] In contrast to pH-sensitive nanocarriers that promote drug release in endosomes, redox-responsive nanoparticles are intended to disassemble and

Received: November 28, 2013
Revised: January 24, 2014
Published: January 27, 2014

 © 2014 American Chemical Society

Scheme 1. Illustration of Disulfide-Linked Glyco-Nanoparticles (SS-GNs) for Hepatoma-Targeting Intracellular Delivery of Anticancer Drugs[a]

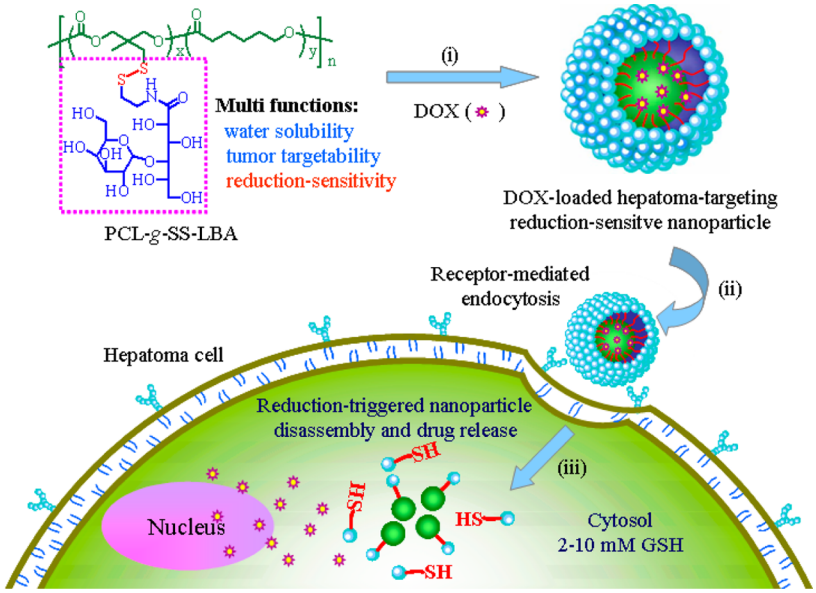

[a](i) SS-GNs are readily obtained from self-assembly of PCL-*g*-SS-LBA graft copolymer; (ii) SS-GNs are efficiently taken up by hepatocellular carcinoma cells via the receptor-mediated mechanism; and (iii) SS-GNs quickly release payloads into the cytosols and cell nuclei due to shedding of saccharide shells.

release drugs into the cytosol that contains about 100- to 1000-fold higher concentration of reducing glutathione (GSH) tripeptide than the extracellular fluids.[23,24] In the past several years, reduction-sensitive nanoparticles containing disulfide linkage(s) in the main chain,[25−27] at the side chain,[28−32] or in the cross-linker[33−35] have been intensively explored for enhanced intracellular drug release. It should be noted, however, that reduction-sensitive nanoparticulate drug formulations caused in general lower in vitro antitumor activity as compared to free drug likely due to inferior uptake by tumor cells.

In this paper, we report on novel disulfide-linked glyco-nanoparticles (SS-GNs) that quickly shed off saccharide shells under an intracellular-mimicking reductive environment as a unique and potent platform for hepatoma-targeting delivery of doxorubicin (DOX; Scheme 1). SS-GNs are obtained with virus sizes from self-assembly of amphiphilic poly(ε-caprolactone)-*graft*-SS-lactobionic acid (PCL-*g*-SS-LBA) graft copolymer. The results show that SS-GNs exhibit good colloidal stability, significantly accelerated drug release in response to 10 mM dithiothreitol (DTT), fast delivery of DOX into the nuclei of liver cancer cells, and superior antitumor activity to free drug.

EXPERIMENTAL SECTION

Materials. Triethylamine (Et_3N, 99%, Alfa Aesar), dithiothreitol (DTT, 99%, Merck), lactobionic acid (LBA, 97%, Acros), stannous octoate ($Sn(Oct)_2$, 95%, Sigma), and doxorubicin hydrochloride (DOX·HCl, 99%, Beijing Zhong Shuo Pharmaceutical Technology Development Co. Ltd.) were used as received. ε-Caprolactone (ε-CL, 99%, Alfa Aesar) was dried over CaH_2 and distilled under reduced pressure prior to use. Toluene was dried by refluxing over sodium wire under an argon atmosphere prior to distillation. Isopropanol was dried by refluxing over CaH_2 under an argon atmosphere. Acryloyl cyclic carbonate monomer (AC) and pyridyldisulfide cyclic carbonate monomer (PDSC) were synthesized according to our previous reports.[36,37]

Characterization. ^1H NMR spectra were recorded on a Unity Inova 400 spectrometer operating at 400 MHz. $CDCl_3$ and DMSO-d_6 were used as solvents and the chemical shifts were calibrated against residual solvent signals. The molecular weight and polydispersity of the copolymers were determined by a Waters 1515 gel permeation chromatograph (GPC) instrument equipped with two linear PLgel columns following a guard column and a differential refractive-index detector. The measurements were performed using $CHCl_3$ as the eluent at a flow rate of 0.5 mL/min at 30 °C and a series of narrow polystyrene standards for the calibration of the columns.

Synthesis of Thiolated Lactobionic Acid (LBA-SH). To a stirred solution of lactobionic acid (LBA, 3 g, 8.37 mmol) in deionized water (20 mL) was added EDC (3.2 g, 16.74 mmol) and NHS (1.9 g, 16.74 mmol). The pH of the solution was adjusted to 5 and then the solution was stirred for 4 h at room temperature. Under a N_2 atmosphere, 2-mercaptoethylamine hydrochloride (2.4 g, 20.93 mmol) was added into the mixture and the pH of the solution was adjusted to 7.4 by an aqueous solution of sodium hydroxide (1 M). The reaction was allowed to proceed for another 24 h. The solution was then treated with DTT (2.0 g, 12.98 mmol) for 5 h. The crude product was isolated by precipitation in isopropanol and washed with methanol to yield LBA-SH. The thiol functionality was determined via the Ellman assay (functionality of SH = 80%).

Synthesis of P(CL-*co*-PDSC) and P(CL-*co*-AC) Functional Copolymers. The ring-opening copolymerization of ε-CL with PDSC or AC was carried out in toluene at 100 °C using $Sn(Oct)_2$ as a catalyst and isopropanol as an initiator. The following is a typical example of the synthesis of P(CL-*co*-PDSC) copolymer. In the glovebox under a N_2 atmosphere, to a stirred solution of ε-CL (42 mg, 0.369 mmol), PDSC (400 mg, 1.476 mmol) and isopropanol (60 μmol) in toluene (4 mL) was quickly added $Sn(Oct)_2$ stock solution (20 mg, 50 μmol). The reaction vessel was sealed and placed in an oil bath thermostatted at 100 °C. The polymerization was allowed to proceed with magnetic stirring for 24 h and terminated by acetic acid. The P(CL-*co*-PDSC) copolymer was isolated by precipitation from cold diethyl ether and dried under vacuum at room temperature. AC-functionalized PCL copolymer was synthesized in a similar method.

Synthesis of PCL-*g*-SS-LBA and PCL-*g*-LBA Graft Copolymers. To a solution of P(CL-*co*-PDSC) (50 mg, 0.144 mmol of PDS group) and LBA-SH (375 mg, 0.72 mmol of SH group) in DMSO (25

dx.doi.org/10.1021/bm401749t | *Biomacromolecules* 2014, 15, 900−907

mL) under a N_2 atmosphere was added a catalytic amount of acetic acid, and the reaction was allowed to proceed with magnetic stirring for 48 h at 40 °C. The reaction was monitored by determining the amount of pyridinethione using UV analysis. The polymer solution was purified by dialysis against deionized water with a molecular weight cutoff (MWCO) of 3500 at room temperature for 48 h, to remove excess LBA-SH and pyridinethione. The product was finally freeze-dried.

PCL-*g*-LBA graft copolymer was synthesized in a similar method by Michael-type conjugate addition reaction in DMSO at room temperature in the presence of a catalytic amount of Et_3N.

Nanoparticle Formation and Critical Aggregation Concentration (CAC). PCL-*g*-SS-LBA and PCL-*g*-LBA copolymer nanoparticles (denoted as SS-GNs and NSS-GNs, respectively) were prepared by the solvent exchange method. In a typical example, to a stirred DMSO solution (200 μL) of PCL-*g*-SS-LBA (5.0 mg/mL) was dropwise added 2.0 mL of phosphate buffer (PB, 10 mM, pH 7.4), and then the mixture was dialyzed against PB (10 mM, pH 7.4) for 8 h with a MWCO of 3500 at room temperature to remove the organic solvent. The size of the nanoparticles was determined using dynamic light scattering (DLS) and transmission electron microscopy (TEM). Suspensions of the nanoparticles were filtered through a 450 nm syringe filter before measurements. Measurements were carried out at 25 °C using a Zetasizer Nano-ZS from Malvern Instruments equipped with a 633 nm He−Ne laser using backscattering detection. TEM was performed using a Tecnai G220 TEM operated at an accelerating voltage of 200 kV. The samples were prepared by dropping 10 μL of a 0.2 mg/mL suspension of the nanoparticles on the copper grid followed by staining with phosphotungstic acid.

The critical aggregation concentration (CAC) was determined using pyrene as a fluorescence probe. The concentration of the polymeric nanoparticles was varied from 2.0×10^{-5} to 0.5 mg/mL and the concentration of pyrene was fixed at 1.0×10^{-6} M. Fluorescence spectra were recorded using a FLS920 fluorescence spectrometer and an excitation wavelength of 330 nm. Fluorescence emissions at 372 and 383 nm were monitored. The CAC was estimated as the cross-point when extrapolating the intensity ratio I_{372}/I_{383} at low and high concentration regions.

Reduction-Triggered Change of Nanoparticle Sizes. The change of nanoparticle sizes in response to 10 mM DTT was followed by DLS measurements at 37 °C. Samples with a polymer concentration of 0.5 mg/mL were prepared as above-mentioned. A suspension of SS-GNs (0.5 mg/mL) was divided into two aliquots of 1 mL, and 10 μL of DTT solution (1.0 M) was added into one of the two aliquots with a final DTT concentration of 10 mM. The samples were slowly stirred at 37 °C under a N_2 atmosphere and the change in the nanoparticle size was monitored over time by DLS. Similar experiments were carried out with reduction-insensitive NSS-GNs (0.5 mg/mL).

Loading and Triggered Release of DOX. DOX was loaded into nanoparticles by dropwise addition of 5.0 mL PB (10 mM, pH 7.4) to a mixture of 500 μL of copolymer solution in DMSO (5 mg/mL) and 25, 50, or 100 μL of DOX solution in DMSO (5.0 mg/mL) under stirring at room temperature, followed by ultrasonication for 0.5 h and dialysis against PB (10 mM, pH 7.4) with a MWCO of 3500 at room temperature in the dark for 8 h. The dialysis medium was changed every hour.

The release profiles of DOX from nanoparticles were determined in PB (100 mM, pH 7.4) at 37 °C either with or without 10 mM DTT. The above prepared DOX-loaded nanoparticle suspensions (containing 0.5 mg/mL nanoparticles and 25 μg/mL DOX) were divided into two aliquots. Each aliquot was immediately transferred to a dialysis tube with a MWCO of 12000−14000. The dialysis tube was immersed into 20 mL of the appropriate buffer and the media were shaken at 37 °C. At desired time intervals, 5 mL of the release medium was taken out for measuring the fluorescence and replenished with an equal volume of fresh medium. To avoid oxidation of DTT, the release media were perfused with nitrogen gas. The concentration of DOX was determined by fluorescence (FLS920) measurements (excitation at 480 nm). For determination of the drug loading content, DOX-loaded nanoparticle suspensions were freeze-dried, then dissolved in DMSO and analyzed with fluorescence spectroscopy. A calibration curve was obtained using DOX/DMSO solutions with different DOX concentrations. To determine the amount of DOX released, calibration curves were run with DOX/phosphate buffer solutions with different DOX concentrations at pH 7.4. The emission at 480 nm was recorded. Release experiments were conducted in triplicate. The results are presented as the average ± standard deviation.

Drug loading content (DLC) and drug loading efficiency (DLE) were calculated according to the following formula:

$$\mathrm{DLC(wt\%)} = (\text{weight of loaded drug/total weight of polymer and loaded drug}) \times 100\%$$

$$\mathrm{DLE(\%)} = (\text{weight of loaded drug/weight of drug in feed}) \times 100\%$$

CLSM of HepG2 Cells Incubated with DOX-Loaded Nanoparticles. HepG2 cells were plated on microscope slides in a 24-well plate (5×10^4 cells/well) using DMEM medium containing 10% FBS. After 24 h incubation, the medium was replaced by 450 μL of fresh DMEM and 50 μL of prescribed amounts of DOX-loaded nanoparticles or free DOX. To confirm that glyco-nanoparticles were taken up by the ASGP-R overexpressing HepG2 cells via a receptor-mediated endocytosis mechanism, 100 μL of free LBA (10 mg/mL) was added 4 h before the addition of DOX-loaded nanoparticles to block ASGP-R on the surface of the HepG2 cells. After incubation for 4 h with the DOX-loaded nanoparticles or free DOX, the culture medium was removed and the cells on microscope plates were washed three times with PBS. The cells were fixed with 4% paraformaldehyde and the cell nuclei were stained with DAPI. Fluorescence images of cells were obtained with Confocal Laser Scanning Microscope (Leica, TCS-SP2).

Flow Cytometry Assay. HepG2 cells were seeded onto 6-well plates at 1×10^5 cells per well for 24 h using DMEM medium containing 10% FBS. After 24 h incubation, the medium was replaced by 0.9 mL of fresh DMEM and 0.1 mL of prescribed amounts of DOX-loaded nanoparticles or free DOX. Similarly, to investigate whether nanoparticles were specifically taken up by HepG2 cells through ASGP-R mediated endocytosis, cells were incubated with free-LBA (2 mg/mL) for 4 h before the addition of DOX-loaded nanoparticles. After incubation at 37 °C for 4 h, the cells were digested by 0.25 w/v% trypsin/0.03 w/v% EDTA. The suspensions were centrifuged at 1500 rpm for 5 min at 25 °C, pelleted in eppendorf tubes, washed twice with cold PBS, and then resuspended in 500 μL of PBS. Fluorescence histograms were recorded with a BD FACSCalibur (Beckton Dickinson) flow cytometer and analyzed using Cell Quest software. We analyzed 10000 gated events to generate each histogram. The gate was arbitrarily set for the detection of DOX fluorescence.

MTT Assay. The cytotoxicity of blank or DOX-loaded nanoparticles was studied by the MTT assays using HepG2 cells and MCF-7 cells. Cells were seeded onto a 96-well plate at a density of 1×10^4 cells per well in 100 μL of Dulbecco's Modified Eagle medium (DMEM) containing 10% FBS and incubated for 24 h (37 °C, 5% CO_2). The medium was replaced by 90 μL of fresh DMEM medium containing 10% FBS, and then 10 μL samples of various concentrations of the nanoparticle suspensions in PB (10 mM, pH 7.4) were added. The cells were incubated for another 48 h, and then 10 μL of MTT solution (5 mg/mL) was added. The cells were incubated for 4 h, and the medium was aspirated and replaced by 150 μL of DMSO to dissolve the resulting purple crystals. The optical densities at 570 nm were measured using a BioTek microplate reader. Cells cultured in DMEM medium containing 10% FBS (without exposure to nanoparticles) were used as controls.

To evaluate whether the high drug efficacy was specially caused by ASGP-R mediated endocytosis, HepG2 cells seeded in a 96-well plate at a density of 1×10^4 cells per well for 24 h were incubated with free LBA (+LBA, 2 mg/mL) or without free LBA (−LBA) 4 h before the addition of DOX-loaded nanoparticles or free DOX. The ASGP-R on

HepG2 cell surface can be blocked in DMEM medium containing free LBA. The cytotoxicity studies for DOX-loaded SS-GNs, DOX-loaded NSS-GNs, and free DOX (drug dosage: 10 μg/mL) were carried out in a similar way. The medium was replaced by 90 μL of fresh DMEM medium and 10 μL of DOX-loaded nanoparticles or free DOX. After an additional 4 h incubation, the medium was replaced by 100 μL of fresh DMEM medium and the cells were cultured for another 48 h. After that, the same procedure was carried out as above-mentioned. A total of 10 μL of MTT solution (5 mg/mL) was added and the cells were incubated for 4 h. The culture medium was aspirated and replaced by 150 μL of DMSO to dissolve the resulting purple crystals. The optical densities at 570 nm were measured using a BioTek microplate reader. Cells cultured in DMEM medium containing 10% FBS (without exposure to nanoparticles) were used as controls.

RESULTS AND DISCUSSION

Synthesis of PCL-*g*-SS-LBA Graft Copolymer. PCL-*g*-SS-LBA graft copolymer was synthesized by ring-opening copolymerization of ε-caprolactone (ε-CL) and pyridyl disulfide carbonate (PDSC) followed by postpolymerization modification with thiolated lactobionic acid (LBA-SH) via the thiol-disulfide exchange reaction (Scheme 2). The copolymerization was carried out for 24 h in toluene at 100 °C using $Sn(Oct)_2$ as a catalyst and isopropanol as an initiator. ^{1}H NMR spectrum showed signals attributable to both CL (δ 4.04, 2.30, 1.64, and 1.38) and PDSC units (δ 8.48, 7.70, 7.12, 4.05, 3.02, and 1.10; Figure S1A). The comparison of signal intensities at δ 3.02 (methylene protons next to the disulfide bond in PDSC units) and 2.30 (methylene protons next to the carbonyl in CL units) showed that P(CL-*co*-PDSC) contained approximately 60.4 mol % PDSC, which was close to the design (Table 1). The number-average molecular weight (M_n) estimated from ^{1}H NMR end group analysis by comparing the integrals of peaks at 2.30 (methylene protons next to carbonyl in CL units) and 3.02 (methylene protons next to the disulfide bond in PDSC units) with δ 4.34 (methine protons of isopropyl ester end group) was 6.4 kg/mol, close to the theoretical value (Table 1). Gel permeation chromatography (GPC) showed that thus obtained P(CL-*co*-PDSC) copolymer had a moderate polydispersity (PDI) of 1.58 and an M_n of 6.9 kg/mol, in agreement with that determined by ^{1}H NMR end group analysis.

Scheme 2. Synthesis of PCL-*g*-SS-LBA Graft Copolymer by Combining Ring-Opening Polymerization and Thiol-Disulfide Exchange Reaction[a]

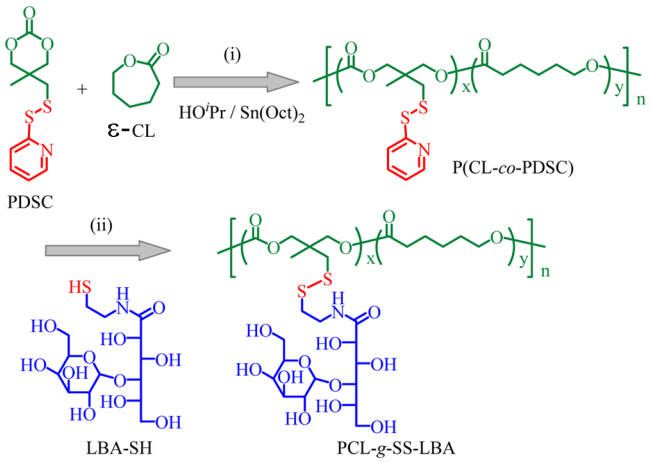

[a]Reagents and conditions: (i) toluene, 100 °C, 24 h; (ii) DMSO, 40 °C, 48 h.

The postpolymerization modification of P(CL-*co*-PDSC) was performed at a LBA-SH/PDS molar ratio of 5/1 in DMSO at 40 °C for 48 h using a catalytic amount of acetic acid (Scheme 2). UV spectroscopy showed quantitative generation of pyridinethione,[38] indicating that LBA has been successfully grafted to PCL. ^{1}H NMR revealed that signals assignable to LBA were detected at δ 3.4−3.8 and 4.4−5.4, while signals at δ 8.48, 7.70, and 7.12 owing to pyridine protons disappeared (Figure S2). It is evident, therefore, that PCL-*g*-SS-LBA graft copolymers can be readily prepared from PDS-functionalized PCL via the thiol-disulfide exchange reaction, through which we have successfully prepared poly(ε-caprolactone)-*g*-SS-poly(ethylene glycol) (PCL-*g*-SS-PEG).[37] Here, we have also synthesized PCL-*g*-LBA as a reduction-insensitive control via ring-opening copolymerization of ε-CL and acryloyl cyclic carbonate (AC) followed by Michael-type addition with LBA-SH, as our previous report (Scheme S1).[36] ^{1}H NMR showed that P(CL-*co*-AC) copolymer had about 62.2 mol % AC units (Figure S1B). GPC revealed that P(CL-*co*-AC) copolymer had a moderate PDI of 1.46 and an M_n of 5.8 kg/mol, close to that of P(CL-*co*-PDSC) (Table 1). The treatment of P(CL-*co*-AC) with LBA-SH resulted in complete vanishing of signals attributable to the acryloyl protons, supporting quantitative conjugation of LBA via Michael-type addition reaction.

Preparation and Reduction-Triggered Dissociation of Glyco-Nanoparticles. Glyco-nanoparticles were readily prepared by the solvent exchange method. The dynamic light scattering (DLS) measurements showed that PCL-*g*-SS-LBA formed monodisperse nanoparticles (SS-GNs) with an average size of approximately 80 nm (Figure 1A). Transmission electron microscopy (TEM) revealed that these nanoparticles had a spherical morphology and a particle size comparable to that determined by DLS (Figure 1B). Similarly, PCL-*g*-LBA formed nanoparticles (NSS-GNs) with an average diameter of about 100 nm (Figure 1A). The fluorescence measurements using pyrene as a probe showed that PCL-*g*-SS-LBA and PCL-*g*-LBA had low critical aggregation concentrations (CACs) of 4.63 and 4.25 mg/L, respectively.

Table 1. Synthesis of Biodegradable P(CL-*co*-PDSC) and P(CL-*co*-AC) Copolymers[a]

					M_n (kg/mol)			
entry	copolymer	[M]/[I]	f^b (%)	F^c (%)	design[d]	^{1}H NMR[e]	GPC[f]	PDI GPC[f]
1	P(CL-*co*-PDSC)	30	70	60.4	6.7	6.4	6.9	1.58
2	P(CL-*co*-AC)	30	70	62.2	5.2	5.8	6.7	1.46

[a]The ring-opening copolymerization was carried out in toluene at 100 °C using isopropanol as an initiator and $Sn(Oct)_2$ as a catalyst. [b]Molar ratio of functional monomers (PDSC or AC) in feed. [c]Molar fraction of functional units determined by ^{1}H NMR. [d]Calculated by the following formulus: $M_n = M_{n(CL)} \times ([M]/[I]) \times (1 - f) + M_{n(PDSC\ or\ AC)} \times ([M]/[I]) \times f$. [e]Determined by end group analysis. [f]Determined by GPC (eluent: chloroform, flow rate: 0.5 mL/min, standards: polystyrene).

dx.doi.org/10.1021/bm401749t | Biomacromolecules 2014, 15, 900−907

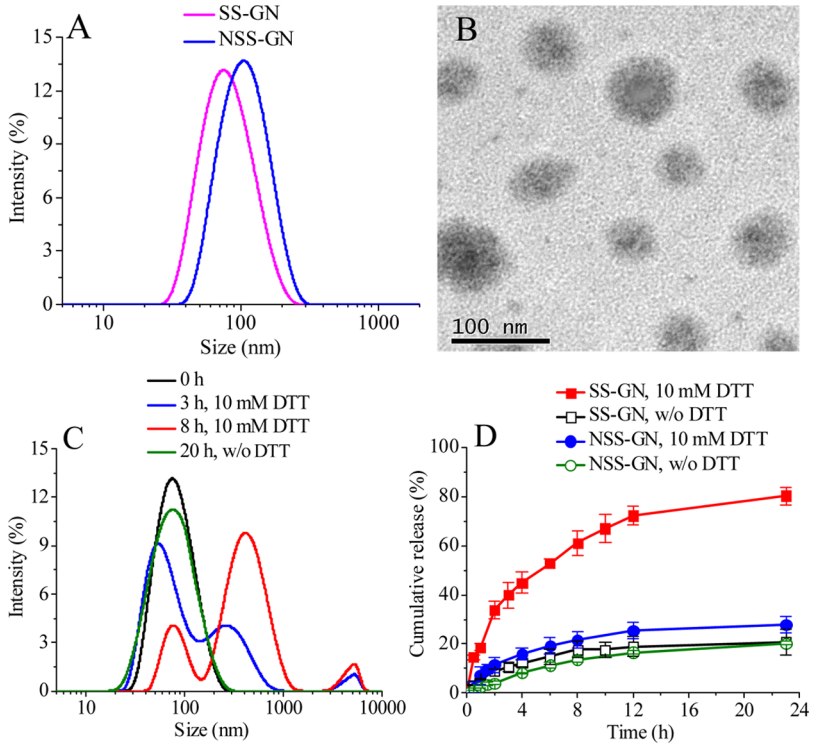

Figure 1. (A) Size distributions of SS-GNs and NSS-GNs determined by DLS; (B) TEM image of SS-GNs; (C) Size change of SS-GNs in response to a reductive environment (10 mM DTT) followed by DLS measurement; and (D) Cumulative release of DOX from SS-GNs in the absence or presence of 10 mM DTT at 37 °C in PB (pH 7.4, 10 mM); NSS-GNs were used as reduction-insensitive control.

The size change of SS-GNs in response to 10 mM DTT (intracellular-mimicking reducing environment) was followed by DLS. Interestingly, these nanoparticles quickly formed large aggregates, in which nanoparticle sizes increased from 80 to 300 nm in 3 h, reaching over 500 nm after 8 h (Figure 1C). In contrast, little size change was observed in 20 h for SS-GNs in the absence of DTT (Figure 1C) as well as for NSS-GNs nanoparticles (reduction-insensitive control) in the presence of 10 mM DTT (Figure S3). The fast aggregation of SS-GNs under a reducing condition is most probably due to reductive cleavage of the intermediate disulfide bonds, which results in shedding of LBA shells.

Loading and Reduction-Triggered Release of DOX. DOX-loaded nanoparticles were prepared by dialysis of a polymer/DOX solution in DMSO against PB (pH 7.4, 10 mM). The results showed that SS-GNs and NSS-GNs exhibited similar DOX loading levels (Table 2). The drug loading efficiencies (DLE) were more than 50% even at a high theoretical drug loading content (DLC) of 20 wt %. The particle sizes increased with increasing DOX loading levels while PDI remained low. At the same DLC, DOX-loaded SS-GN was somewhat smaller than DOX-loaded NSS-GN, which is most likely due to the different linker structure between PCL and LBA. The in vitro release of DOX from SS-GNs was investigated using a dialysis tube (MWCO 12000−14000) in PB (pH 7.4, 100 mM) with or without 10 mM DTT. To avoid the precipitation of DOX due to fast release, drug release studies were performed at a low DLC of 4.7 wt % and with 0.5 mL of DOX-loaded nanoparticle suspension (0.5 mg/mL) dialysis against 20 mL of the same medium. The results showed that SS-GNs released DOX rapidly in the presence of 10 mM DTT, in which about 52.7 and 72.2% of DOX was released in 6 and 12 h, respectively (Figure 1D). In contrast, minimal drug release (less than 30% in 24 h) was observed for SS-GNs under nonreducing environment as well as for reduction-insensitive NSS-GNs either in the presence or absence of 10 mM DTT. Notably, in all cases, no burst drug release was observed. This is in line with the previous reports that shell-sheddable micelles are able to rapidly release DOX under reductive conditions.[39−42]

Table 2. DOX Loading Content and Loading Efficiency of Glyco-Nanoparticles

	DLC (wt%)				
nanoparticles	theory	determined[a]	DLE (%)	size[b] (nm)	PDI[b]
SS-GN	5	2.5	50.1	85.2 ± 1.4	0.16
	10	5.8	56.0	92.4 ± 1.5	0.18
	20	12.0	55.0	105.3 ± 3.2	0.22
NSS-GN	5	2.6	51.2	113.6 ± 2.6	0.21
	10	5.4	50.8	126.4 ± 2.4	0.19
	20	11.5	53.5	140.7 ± 3.5	0.26

[a]Determined by fluorescence measurements. [b]Determined by DLS measurements.

Hepatoma-Targeting Intracellular Release of DOX. To evaluate the targetability of these glyco-nanoparticles to liver tumor cells, cellular DOX levels were studied in ASGP-R overexpressing HepG2 cells using flow cytometry. Notably, HepG2 cells following a 4 h incubation with DOX-loaded SS-GNs revealed high cellular DOX levels (Figure 2A), which was approximately 10-fold higher than that for HepG2 cells pretreated with LBA (+LBA; Figure S4A), supporting that cellular uptake of DOX-loaded SS-GNs via ASGP-R receptor mediated endocytosis mechanism. It should further be noted that cellular DOX level in HepG2 cells (−LBA) after 4 h

dx.doi.org/10.1021/bm401749t | Biomacromolecules 2014, 15, 900−907

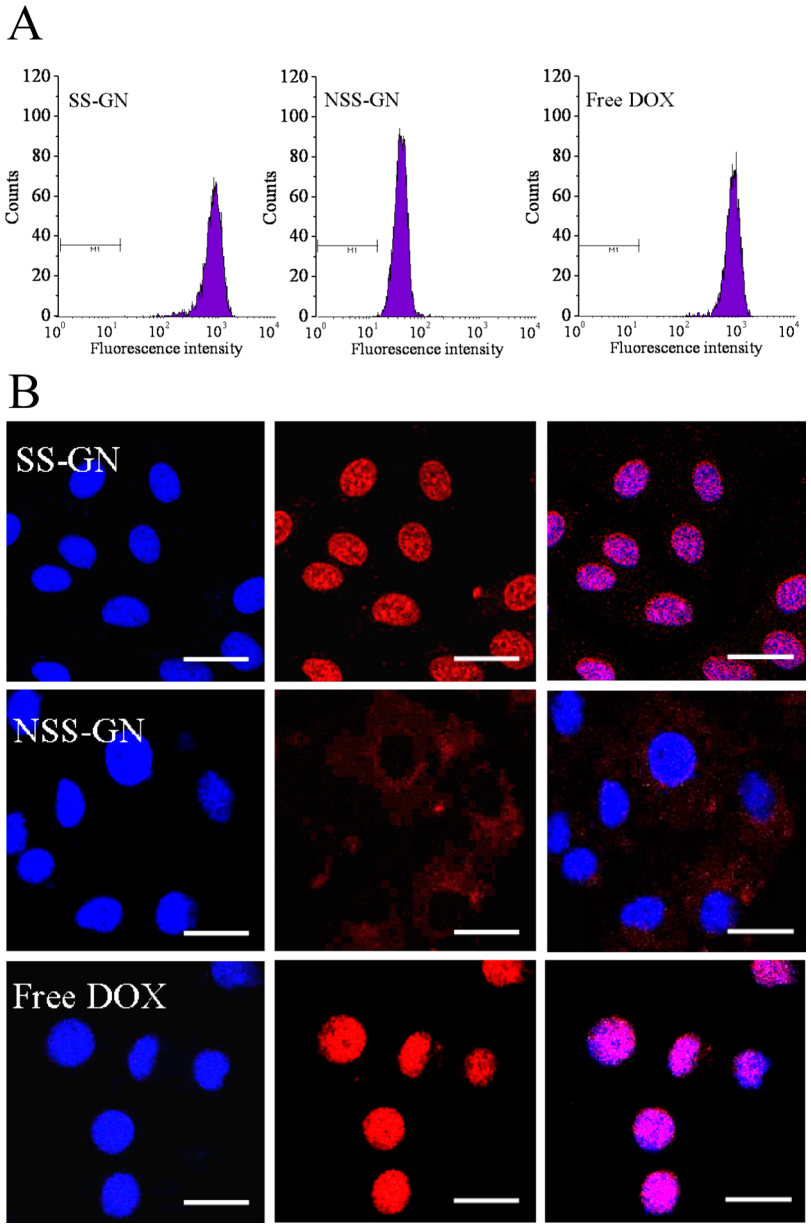

Figure 2. Cellular uptake and intracellular release of DOX into HepG2 cells following 4 h incubation. (A) Flow cytometric analysis. Cells were treated for 4 h with DOX-loaded nanoparticles or free DOX (dosage: 5 μg/mL, cell counts: 10000). (B) CLSM images of HepG2 cells incubated with DOX-loaded nanoparticles or free DOX (5 μg/mL). For each panel, the images from left to right show cell nuclei stained by DAPI (blue), DOX fluorescence in cells (red) and overlays of the two images. The scale bars correspond to 25 μm in all the images.

incubation with DOX-loaded SS-GNs was more than 20 times higher than that for cells treated with DOX-loaded NSS-GNs under otherwise the same conditions (Figure 2A). Given the fact that SS-GNs and NSS-GNs had similar particle sizes and LBA densities, the low cellular DOX level observed for HepG2 cells treated with DOX-loaded NSS-GNs is most likely due to comparably slow DOX release inside cells. These results suggest that SS-GNs have elegantly addressed both cellular uptake and intracellular drug release issues. It is interesting to note that HepG2 cells following incubation with DOX-loaded SS-GNs exhibited similar cellular DOX levels to those with free DOX (Figure 2A).

To further investigate the cellular distribution of DOX, HepG2 cells following incubation with DOX-loaded SS-GNs were further studied using confocal laser scanning microscopy (CLSM). Remarkably, cells following 4 h incubation with DOX-loaded SS-GNs displayed strong DOX fluorescence in their nuclei, which is similar to those treated with free DOX under otherwise the same conditions (Figure 2B). In sharp contrast, little DOX fluorescence was observed in cells pretreated with LBA (+LBA) (Figure S4B) as well as in cells treated with DOX-loaded reduction-insensitive NSS-GNs (Figure 2B). These shell-sheddable glyco-nanoparticles, therefore, provide an effective approach for rapid translocation of drug into the nuclei of hepatocellular carcinoma cells. The high hepatoma-targetability of SS-GNs is likely associated with the cluster glycoside effect.[16] The fast release of drug to the nuclei indicates that SS-GNs can efficiently bypass or escape from endosomes. The exact mechanism is not clear and warrants further investigation.

Antitumor Activity of DOX-Loaded Glyco-Nanoparticles. MTT assays using ASGP-R positive HepG2 cells and

dx.doi.org/10.1021/bm401749t | *Biomacromolecules* 2014, 15, 900−907

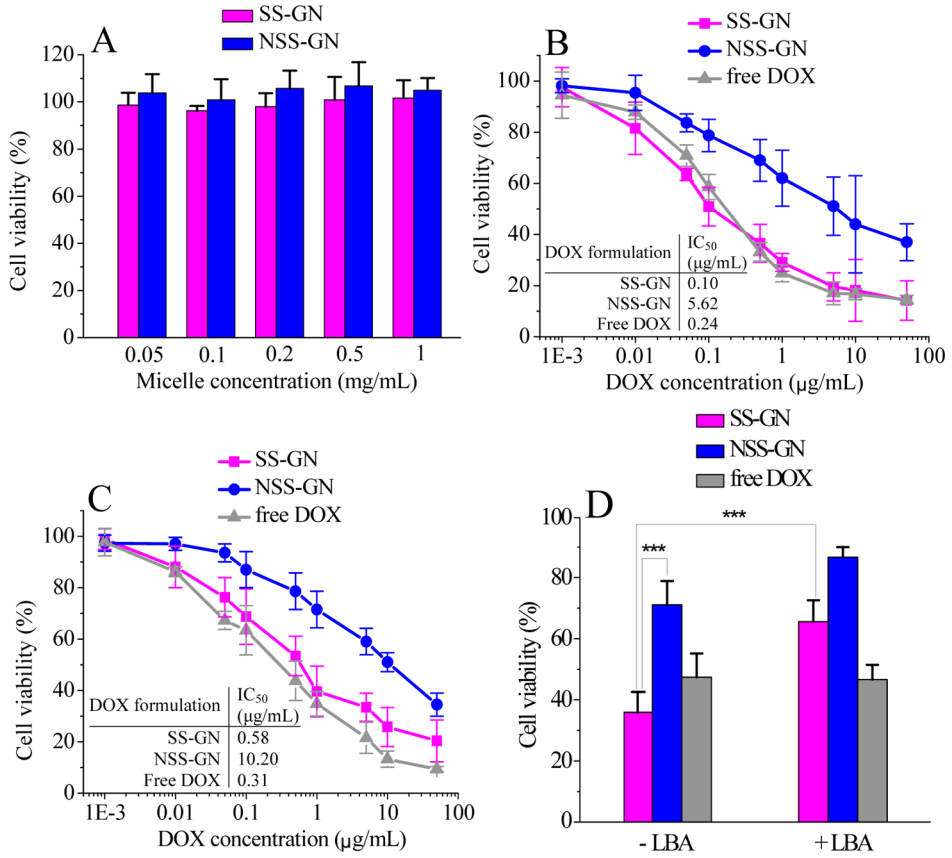

Figure 3. Antitumor activity of DOX-loaded glyco-nanoparticles in HepG2 cells using MTT assays. (A) Cytotoxicity of blank glyco-nanoparticles at different concentrations by MTT assays using HepG2 cells following 48 h incubation; (B, C) Cell viability of HepG2 and MCF-7 cells following 48 h incubation with DOX-loaded glyco-nanoparticles and free DOX at varying DOX concentrations from 1.0×10^{-3} to 50 μg/mL, respectively; (D) Competitive inhibition experiments. HepG2 cells were cultured for 4 h without (−LBA) or with LBA (+LBA), then the medium was replaced by 80 uL of fresh DMEM medium and 20 μL of DOX-loaded nanoparticles or free DOX. DOX dosage was 10 μg/mL. After a 4 h incubation, the medium was replaced by 100 μL of fresh DMEM medium and the cells were cultured for another 48 h. Data are presented as the average ± standard deviation (n = 4, Student's t test, ***p < 0.001).

ASGP-R negative MCF-7 cells revealed that both SS-GNs and NSS-GNs were practically nontoxic (cell viabilities ≥95%) up to a tested concentration of 1.0 mg/mL (Figures 3A and S5), confirming that these glyco-nanoparticles have good biocompatibility. Notably, DOX-loaded SS-GNs exhibited superior antitumor activity to DOX-loaded NSS-GNs counterparts in both HepG2 and MCF-7 cells (Figure 3B,C). For example, the half maximal inhibitory concentration (IC_{50}) of DOX-loaded SS-GNs toward HepG2 cells was determined to be 0.10 μg DOX equiv/mL, which was about 56-fold lower than reduction-insensitive NSS-GNs under otherwise the same conditions (IC_{50} = 5.6 μg DOX equiv/mL). The high antitumor efficacy of DOX-loaded SS-GNs is likely due to their fast DOX release under the intracellular reductive conditions. Moreover, DOX-loaded SS-GNs were substantially more potent to HepG2 cells than to MCF-7 cells (IC_{50}: 0.10 vs 0.58 μg DOX equiv/mL), confirming that SS-GNs possess apparent targetability to ASGP-R overexpressing HepG2 cells. It is remarkable to note that DOX-loaded SS-GNs exhibited even better therapeutic effects in HepG2 cells than free DOX at low concentrations (IC_{50} = 0.24 μg/mL).

To further study hepatoma-targetability and antitumor activity of SS-GNs, HepG2 cells were incubated only for 4 h with DOX-loaded nanoparticles. The culture medium was removed and replenished with fresh culture medium and the cells were cultured for another 48 h. Interestingly, HepG2 cells treated with DOX-loaded SS-GNs displayed a low cell viability of 35.9%, which was much lower than those incubated with DOX-loaded reduction-insensitive NSS-GN counterparts (cell viability: 71.0%) as well as free DOX (cell viability: 47.5%) under otherwise the same conditions (Figure 3D). The competitive inhibition experiments showed that cell viability of HepG2 cells increased from 35.9 to 65.5% following pretreating with LBA (Figure 3D), confirming that DOX-loaded SS-GNs are taken up by HepG2 cells via a receptor-mediated mechanism. It is evident, therefore, that these reduction-sensitive shell-sheddable glyco-nanoparticles possess high targetability and superior in vitro therapeutic activity toward liver cancer cells.

CONCLUSIONS

We have demonstrated for the first time that disulfide-linked glyco-nanoparticles can efficiently deliver and release anticancer drugs into the hepatocellular carcinoma cells, presenting excellent hepatoma-targetability and superior in vitro antitumor activity to free drugs. The saccharide shells have uniquely integrated multifunctions such as biocompatibility, water solubility, tumor-targetability, and reduction-sensitivity. These reduction-sensitive glyco-nanoparticles provide a potent platform for targeted liver cancer chemotherapy. It should further be noted that this study presents a general strategy, that is, grafting water-soluble targeting ligands to degradable polymer

dx.doi.org/10.1021/bm401749t | Biomacromolecules 2014, 15, 900−907

backbone via a stimuli-sensitive cleavable bond, to construct tumor-targeting and virus-mimicking multifunctional drug delivery systems.

■ ASSOCIATED CONTENT

Supporting Information

Synthesis of PCL-*g*-LBA graft copolymer, ^{1}H NMR spectra of P(CL-*co*-PDSC), P(CL-*co*-AC), and PCL-*g*-SS-LBA, size distribution of NSS-GNs in response to 10 mM DTT, competitive inhibition experiments using HepG2 cells pretreated for 4 h with free LBA (2 mg/mL), and cytotoxicity of blank glyco-nanoparticles in MCF-7 cells following a 48 h incubation. This material is available free of charge via the Internet at http://pubs.acs.org.

■ AUTHOR INFORMATION

Corresponding Author

*Tel./Fax: +86-512-65880098. E-mail: cdeng@suda.edu.cn (C.D.); zyzhong@suda.edu.cn (Z.Z.).

Notes

The authors declare no competing financial interest.

■ ACKNOWLEDGMENTS

This work was supported by the National Natural Science Foundation of China (NSFC 51003070, 51103093, 51173126, and 51273139), the National Science Fund for Distinguished Young Scholars (51225302), and a Project Funded by the Priority Academic Program Development of Jiangsu Higher Education Institutions.

■ REFERENCES

(1) Haag, R.; Kratz, F. *Angew. Chem., Int. Ed.* **2006**, *45*, 1198−1215.
(2) Davis, M. E.; Chen, Z.; Shin, D. M. *Nat. Rev. Drug Discovery* **2008**, *7*, 771−782.
(3) Schroeder, A.; Heller, D. A.; Winslow, M. M.; Dahlman, J. E.; Pratt, G. W.; Langer, R.; Jacks, T.; Anderson, D. G. *Nat. Rev. Cancer* **2012**, *12*, 39−50.
(4) Deng, C.; Jiang, Y.; Cheng, R.; Meng, F.; Zhong, Z. *Nano Today* **2012**, *7*, 467−480.
(5) Fang, J.; Nakamura, H.; Maeda, H. *Adv. Drug Delivery Rev.* **2011**, *63*, 136−151.
(6) Kataoka, K.; Harada, A.; Nagasaki, Y. *Adv. Drug Delivery Rev.* **2012**, *64*, 37−48.
(7) Riehemann, K.; Schneider, S. W.; Luger, T. A.; Godin, B.; Ferrari, M.; Fuchs, H. *Angew. Chem., Int. Ed.* **2009**, *48*, 872−897.
(8) Jain, R. K.; Stylianopoulos, T. *Nat. Rev. Clin. Oncol.* **2010**, *7*, 653−664.
(9) Lammers, T.; Kiessling, F.; Hennink, W. E.; Storm, G. *J. Controlled Release* **2012**, *161*, 175−187.
(10) Byrne, J. D.; Betancourt, T.; Brannon-Peppas, L. *Adv. Drug Delivery Rev.* **2008**, *60*, 1615−1626.
(11) Bae, Y. H.; Park, K. *J. Controlled Release* **2011**, *153*, 198−205.
(12) Ma, P. a.; Liu, S.; Huang, Y.; Chen, X.; Zhang, L.; Jing, X. *Biomaterials* **2010**, *31*, 2646−2654.
(13) Yang, R.; Meng, F.; Ma, S.; Huang, F.; Liu, H.; Zhong, Z. *Biomacromolecules* **2011**, *12*, 3047−3055.
(14) Zhong, Y.; Yang, W.; Sun, H.; Cheng, R.; Meng, F.; Deng, C.; Zhong, Z. *Biomacromolecules* **2013**, *14*, 3723−3730.
(15) Gabor, F.; Bogner, E.; Weissenboeck, A.; Wirth, M. *Adv. Drug Delivery Rev.* **2004**, *56*, 459−480.
(16) Jayaraman, N. *Chem. Soc. Rev.* **2009**, *38*, 3463−3483.
(17) Becer, C. R. *Macromol. Rapid Commun.* **2012**, *33*, 742−752.
(18) Suriano, F.; Pratt, R.; Tan, J. P. K.; Wiradharma, N.; Nelson, A.; Yang, Y.-Y.; Dubois, P.; Hedrick, J. L. *Biomaterials* **2010**, *31*, 2637−2645.
(19) Fleige, E.; Quadir, M. A.; Haag, R. *Adv. Drug Delivery Rev.* **2012**, *64*, 866−884.
(20) Zhang, Q.; Re, K. N.; Kwon, O. J. *Chem. Commun.* **2012**, *48*, 7542−7552.
(21) Meng, F.; Cheng, R.; Deng, C.; Zhong, Z. *Mater. Today* **2012**, *15*, 436−442.
(22) Cheng, R.; Meng, F.; Deng, C.; Klok, H.-A.; Zhong, Z. *Biomaterials* **2013**, *34*, 3647−3657.
(23) Cheng, R.; Feng, F.; Meng, F.; Deng, C.; Feijen, J.; Zhong, Z. *J. Controlled Release* **2011**, *152*, 2−12.
(24) Sun, H.; Meng, F.; Cheng, R.; Deng, C.; Zhong, Z. *Expert Opin. Drug Delivery* **2013**, *10*, 1109−1122.
(25) Sun, H.; Guo, B.; Cheng, R.; Meng, F.; Liu, H.; Zhong, Z. *Biomaterials* **2009**, *30*, 6358−6366.
(26) Thambi, T.; Yoon, H. Y.; Kim, K.; Kwon, I. C.; Yoo, C. K.; Park, J. H. *Bioconjugate Chem.* **2011**, *22*, 1924−1931.
(27) Wen, H.-Y.; Dong, H.-Q.; Xie, W.-j.; Li, Y.-Y.; Wang, K.; Pauletti, G. M.; Shi, D.-L. *Chem. Commun.* **2011**, *47*, 3550−3552.
(28) Liu, J.; Huang, W.; Pang, Y.; Huang, P.; Zhu, X.; Zhou, Y.; Yan, D. *Angew. Chem., Int. Ed.* **2011**, *50*, 9162−9166.
(29) Sun, P.; Zhou, D.; Gan, Z. *J. Controlled Release* **2011**, *155*, 96−103.
(30) Sun, Y.; Yan, X.; Yuan, T.; Liang, J.; Fan, Y.; Gu, Z.; Zhang, X. *Biomaterials* **2010**, *31*, 7124−7131.
(31) Khorsand, B.; Lapointe, G.; Brett, C.; Oh, J. K. *Biomacromolecules* **2013**, *14*, 2103−2111.
(32) Rahimian-Bajgiran, K.; Chan, N.; Zhang, Q.; Noh, S. M.; Lee, H.-i.; Oh, J. K. *Chem. Commun.* **2013**, *49*, 807−809.
(33) Li, Y.-L.; Zhu, L.; Liu, Z.; Cheng, R.; Meng, F.; Cui, J.-H.; Ji, S.-J.; Zhong, Z. *Angew. Chem., Int. Ed.* **2009**, *48*, 9914−9918.
(34) Dai, J.; Lin, S.; Cheng, D.; Zou, S.; Shuai, X. *Angew. Chem., Int. Ed.* **2011**, *50*, 9404−9408.
(35) Wei, R.; Cheng, L.; Zheng, M.; Cheng, R.; Meng, F.; Deng, C.; Zhong, Z. *Biomacromolecules* **2012**, *13*, 2429−2438.
(36) Chen, W.; Yang, H.; Wang, R.; Cheng, R.; Meng, F.; Wei, W.; Zhong, Z. *Macromolecules* **2010**, *43*, 201−207.
(37) Chen, W.; Zou, Y.; Jia, J.; Meng, F.; Cheng, R.; Deng, C.; Feijen, J.; Zhong, Z. *Macromolecules* **2013**, *46*, 699−707.
(38) Ryu, J.-H.; Chacko, R. T.; Jiwpanich, S.; Bickerton, S.; Babu, R. P.; Thayumanavan, S. *J. Am. Chem. Soc.* **2010**, *132*, 17227−17235.
(39) Sun, H.; Guo, B.; Li, X.; Cheng, R.; Meng, F.; Liu, H.; Zhong, Z. *Biomacromolecules* **2010**, *11*, 848−854.
(40) Chen, W.; Zhong, P.; Meng, F.; Cheng, R.; Deng, C.; Feijen, J.; Zhong, Z. *J. Controlled Release* **2013**, *169*, 171−179.
(41) Wang, Y.-C.; Wang, F.; Sun, T.-M.; Wang, J. *Bioconjugate Chem.* **2011**, *22*, 1939−1945.
(42) Ren, T.-B.; Feng, Y.; Zhang, Z.-H.; Li, L.; Li, Y.-Y. *Soft Matter* **2011**, *7*, 2329−2331.